JYVÄSKYLÄN YLIOPISTO

EFFECTIVE AXIAL-VECTOR COUPLING IN BETA DECAY OF MASS REGION A = 100 - 134 ISOTOPES

Pekka Pirinen
Master's thesis
University of Jyväskylä
Department of physics
Supervisor: Jouni Suhonen
October 2014

Abstract

An extensive evaluation of beta decay properties was made across a vast mass region of $A = 100 - 134$. Triplets of nuclei, consisting of an odd-odd nucleus with a 1^+ ground state and its two neighbouring even-even isobars, were taken under examination in order to better understand the behaviour of the effective axial-vector coupling constant g_A as a function of the mass number A. The need for such an effective value of g_A in the QRPA framework has become evident in recent years but a model for the behaviour of this effective g_A over a specific mass region is an idea little investigated. The calculations in this master's thesis were made in the QRPA framework, using large model spaces and realistic Bonn-A two-body interactions.

The overall behaviour of g_A over the mass region was mapped by fixing the value of g_A for each triplet separately by fitting the geometric mean of the left and right Gamow-Teller matrix elements to an experimental value. This was done with four different values of the pnQRPA particle-particle interaction strength, $g_{pp} = 0.6$, 0.7, 0.8, 0.9, and the resulting values of g_A were plotted as a function of A. By this method a linear model for the effective g_A is proposed and put to a test by predicting $\log ft$ values for ground state to ground state decays as well as decays to the first excited states of the even-even nuclei. A fairly average value of $g_{pp} = 0.7$ was chosen for the predictions.

The linear model for g_A performed very well in predicting the ground state to ground state transitions, yielding a mean deviation of 0.23 from the experimental $\log ft$ values. The decays to the first excited 2^+ states of the even-even nuclei were also decently predicted but the calculated $\log ft$ values of decays to the quadrupole two-phonon triplet states were not as accurate. The mean deviations from experimental values became 0.47 for decays to the 2_1^+ state, 0.74 to the 0_{2-ph}^+ state and 0.82 to the 2_{2-ph}^+ state. Still, the linear model performs much better than any constant value of g_A over this mass region.

Contents

1 Introduction

The axial-vector coupling constant of weak interactions, g_A, is a parameter of utmost interest in the study of single and double beta decays. The value of g_A is normally determined by the partially conserved axial-vector current hypothesis of the standard model [1]. There has recently been a consensus that instead of the usual bare value of $g_A = 1.25$, a quenched effective value of g_A should be used for calculating single and double beta decay matrix elements to better adjust the microscopic theory to reproduce experimental values [2–4].

The transition strengths of beta decay to or from an odd-odd nucleus can be calculated using a neighbouring even-even isobar as a starting point [1]. There are various ways of finding the wave functions of the states in the odd-odd nucleus as well as the excited states of the even-even nucleus, of which the QRPA framework [5] has proven successful with reasonable computational effort. Comparing these transition strengths to experimental data gives information on the systematics of single beta decays and also opens possibilities to theoretically probe the experimentally evasive double beta decay [6].

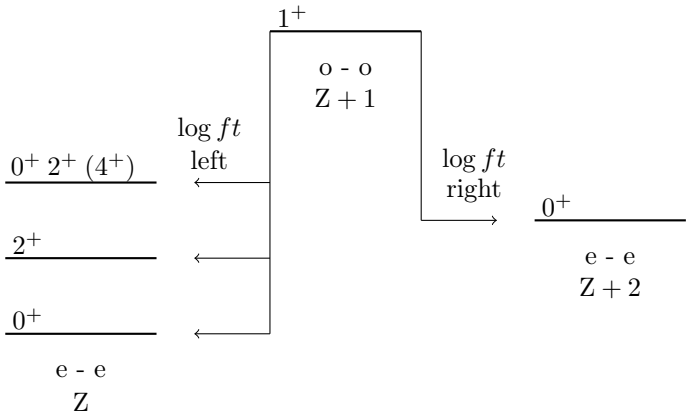

Figure 1: A schematic representation of the decay processes studied in this work. The nucleus in the middle is odd-odd, it's neighbours on the left and right are even-even.

A selection of medium heavy nuclei in the mass region $A = 100 - 134$ are taken under investigation. The nuclei are grouped into triplets where an odd-odd nucleus with a 1^+ ground state is in the "center" and two neighbouring even-even isobars with 0^+ ground states are to the "left" and "right" of the odd-odd nucleus as is represented in Figure 1. Ground state to ground state beta decays as well as decays to excited states of the even-even nuclei are predicted using the QRPA framework.

The situations of Figure 1, where the even-even nuclei on the left and right are lower in energy than the odd-odd nucleus, are particularly of interest as this permits the rare phenomenon of double beta decay [7]. Double beta decay is not discussed further in this master's thesis but the results presented here should be interesting to apply to it's theoretical research.

The purpose of this work is to map the behaviour of g_A over a vast mass region in order to find a suitable model for the effective value of g_A. In Section 2 the required theoretical framework is discussed. In Section 3 the framework is put to good use and based on some initial calculations a linear model for g_A is proposed and adapted for predictions of $\log ft$ values for allowed Gamow-Teller beta decays in the mass region. Finally in Section 4 conclusions are drawn and some final remarks are given regarding application to research of double beta decay.

2 Theoretical background

To effectively describe beta decay transitions between the ground state of an odd-odd nucleus and the ground state and low-lying excited states of an even-even nucleus, one needs to adopt a formalism capable of producing the wave functions of both states involved in the process. The formalism used in this work is the charge conserving quasiparticle random-phase approximation (QRPA) and it's charge non-conserving cousin, the proton-neutron QRPA (pnQRPA). Both the QRPA and the pnQRPA use the BCS quasiparticle theory as a starting point, a theory first introduced by Bardeen, Cooper and Schrieffer in [8]. The BCS theory is discussed in more detail in [1, 9]. The correlated vacuum ground state in the QRPA framework consists of the BCS ground state of an even-even nucleus with small corrections from 4, 8, 12, ... quasiparticle contributions.

2.1 The QRPA

The charge conserving QRPA is used to obtain wave functions and energies of the excited states of even-even nuclei. The wave functions of basic one-phonon excited states in the QRPA are of the form [1]

$$|\omega\rangle_{QRPA} = Q^{\dagger}_{\omega} \, |QRPA\rangle \ . \tag{1}$$

The QRPA phonon creation operator is defined as

$$Q^{\dagger}_{\omega} = \sum_{a \leq b} \left[X^{\omega}_{ab} A^{\dagger}_{ab}(JM) - Y^{\omega}_{ab} \widetilde{A}_{ab}(JM) \right] \ , \tag{2}$$

with the quasiparticle pair creation operator

$$A^{\dagger}_{ab}(JM) = \mathcal{N}_{ab}(J) \left[a^{\dagger}_{a} a^{\dagger}_{b} \right]_{JM}$$

and the time reversed pair annihilation operator

$$\widetilde{A}_{ab}(JM) = -\mathcal{N}_{ab}(J) \left[\widetilde{a}_{a} \widetilde{a}_{b} \right]_{JM} \ .$$

The amplitudes X^{ω}_{ab} and Y^{ω}_{ab} are components of the eigenvectors of a non-Hermitian eigenvalue problem, the matrix form of the so called QRPA equations [1]. These equations can be derived by the equations-of-motion method

first introduced by Rowe in [10]:

$$\begin{bmatrix} \mathrm{A} & \mathrm{B} \\ -\mathrm{B}^* & -\mathrm{A}^* \end{bmatrix} \begin{bmatrix} \mathrm{X}^\omega \\ \mathrm{Y}^\omega \end{bmatrix} = E_\omega \begin{bmatrix} \mathrm{X}^\omega \\ \mathrm{Y}^\omega \end{bmatrix} . \tag{3}$$

The elements of matrices A and B in equation (3) can be explicitly written as [1]

$$\begin{aligned} A_{ab,cd}(J) = {} & (E_a + E_b)\delta_{ac}\delta_{bd} \\ & + G_{pp}(u_a u_b u_c u_d + v_a v_b v_c v_d) \langle a\, b\,;\, J| \, V \, |c\, d\,;\, J\rangle \\ & + G_{ph}\mathcal{N}_{ab}\mathcal{N}_{cd}\big[(u_a v_b u_c v_d + v_a u_b v_c u_d) \langle a\, b^{-1}\,;\, J| \, V_{RES} \, |c\, d^{-1}\,;\, J\rangle \\ & - (-1)^{j_c+j_d+J}(u_a v_b v_c u_d + v_a u_b u_c v_d) \langle a\, b^{-1}\,;\, J| \, V_{RES} \, |d\, c^{-1}\,;\, J\rangle \big] , \end{aligned} \tag{4}$$

$$\begin{aligned} B_{ab,cd}(J) = {} & -G_{pp}(u_a u_b v_c v_d + v_a v_b u_c u_d) \langle a\, b\,;\, J| \, V \, |c\, d\,;\, J\rangle \\ & + G_{ph}\mathcal{N}_{ab}\mathcal{N}_{cd}\big[(u_a v_b v_c u_d + v_a u_b u_c v_d) \langle a\, b^{-1}\,;\, J| \, V_{RES} \, |c\, d^{-1}\,;\, J\rangle \\ & - (-1)^{j_c+j_d+J}(u_a v_b u_c v_d + v_a u_b v_c u_d) \langle a\, b^{-1}\,;\, J| \, V_{RES} \, |d\, c^{-1}\,;\, J\rangle \big] , \end{aligned} \tag{5}$$

where u_i and v_i ($i = a,\ b,\ c,\ d$) are the BCS occupation amplitudes and the normalization factors

$$\mathcal{N}_{ab}(J) = \begin{cases} 1, & \text{for } a \neq b \\ \frac{1}{\sqrt{2}}, & \text{for } a = b\ ,\ J = \text{even} \\ 0, & \text{otherwise} \end{cases} .$$

The particle-hole and particle particle interaction parameters G_{ph} and G_{pp} are discussed in Section 2.3. The matrix A contains contributions from the quasiparticle mean field and the two-quasiparticle-two-quasihole part of the nuclear Hamiltonian. The matrix B contains contributions only from the four-quasiparticle part of the Hamiltonian [1].

The X and Y amplitudes satisfy the orthonormality and completeness relations [1]

$$\sum_{a\le b} \left(X_{ab}^{kJ^\pi *} X_{ab}^{k'J^\pi} - Y_{ab}^{kJ^\pi *} Y_{ab}^{k'J^\pi} \right) = \delta_{kk'} ,$$

$$\sum_{k} \left(X_{ab}^{kJ^\pi} X_{cd}^{kJ^\pi *} - Y_{ab}^{kJ^\pi} Y_{cd}^{kJ^\pi *} \right) = \delta_{ac}\delta_{bd} , \quad a \le b\ ,\ c \le d ,$$

$$\sum_{k} \left(X_{ab}^{kJ^\pi} Y_{cd}^{kJ^\pi *} - Y_{ab}^{kJ^\pi *} X_{cd}^{kJ^\pi} \right) = 0 , \quad a \le b\ ,\ c \le d\ .$$

The non-Hermitian nature of the QRPA matrix equation (3) gives rise to both positive and negative energy solutions [1]. If a triplet E_ω, X^ω, Y^ω is a solution for the matrix equation, then also

$$E_{\omega'} = -E_\omega, \quad \mathrm{X}^{\omega'} = \mathrm{Y}^{\omega *}, \quad \mathrm{Y}^{\omega'} = \mathrm{X}^{\omega *}$$

is a solution. Investigating the squared norm of the negative energy solution gives

$$\begin{aligned} ||\omega_-\rangle|^2 = \langle \omega_- | \omega_- \rangle &= \sum_{ab} \left(\left| X_{ab}^{\omega_-} \right|^2 - \left| Y_{ab}^{\omega_-} \right|^2 \right) \\ &= \sum_{ab} \left(\left| Y_{ab}^{\omega_+} \right|^2 - \left| X_{ab}^{\omega_+} \right|^2 \right) = - \, ||\omega_+\rangle|^2 = -1 \, , \end{aligned} \tag{6}$$

which is a contradiction as a squared norm cannot be negative. As the positive energy solutions already constitute a complete set of eigenstates, the negative energy solutions are discarded as unphysical.

One can use the wave function of a one-phonon state to build a collection of excited two-phonon states with twice the energy of the one-phonon state [1, 6]. The general form of a normalized two-phonon state is [1]

$$|\omega\omega' \, ; \, J \, M\rangle = \frac{1}{\sqrt{1+\delta_{\omega\omega'}}} \left[Q_\omega^\dagger Q_{\omega'}^\dagger \right]_{JM} |QRPA\rangle \ . \tag{7}$$

As the QRPA prediction for the first 2^+ state is often the most accurate, the scope of this work is focused on the triplet of $J^\pi = 0^+$, 2^+, 4^+ states formed of the lowest quadrupole phonon state. The wave functions of these states are, from equation (7)

$$|J^\pi_{2-ph} \, M\rangle = \frac{1}{\sqrt{2}} \left[Q^\dagger(2_1^+) Q^\dagger(2_1^+) \right]_{JM} |QRPA\rangle \ . \tag{8}$$

The existence of such degenerate or, in reality, nearly degenerate two-phonon multiplets is backed by experimental evidence, for example in [11]. A good example of a quadrupole two-phonon triplet is visible in the low energy spectrum of ^{122}Te in Figure 2

2.2 The pnQRPA

The charge-changing proton-neutron variant of the QRPA follows quite straightforwardly from the results of the previous subsection by converting the investigated particles into protons and neutrons. As the regular QRPA permitted the

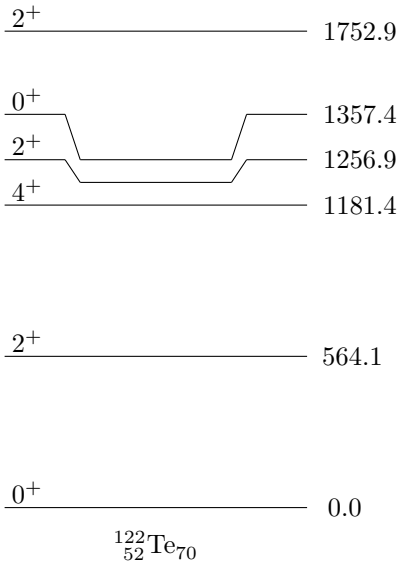

Figure 2: The experimental low energy spectrum of ^{122}Te [12]. The energies are in keV. The quadrupole two-phonon triplet lies around 1200 keV: approximately twice the energy of the lowest 2^+ state.

examination of excited states in even-even nuclei, the pnQRPA is a formalism which describes states of odd-odd nuclei with respect to the even-even QRPA ground state. One can, with no substantial hazard, assume that the QRPA and pnQRPA vacuums coincide in the quasiboson approximation used to describe the β^- and β^+/EC decays [13]. Then, the basic excitations in the pnQRPA can be written as

$$|\omega\rangle_{pnQRPA} = \sum_{pn} \left[X^{\omega}_{pn} A^{\dagger}_{pn}(JM) - Y^{\omega}_{pn} \widetilde{A}_{pn}(JM) \right] |QRPA\rangle \ . \tag{9}$$

The pnQRPA equations are formally exactly the same as the QRPA equations (3):

$$\begin{bmatrix} \mathrm{A} & \mathrm{B} \\ -\mathrm{B}^* & -\mathrm{A}^* \end{bmatrix} \begin{bmatrix} \mathrm{X}^{\omega} \\ \mathrm{Y}^{\omega} \end{bmatrix} = E_{\omega} \begin{bmatrix} \mathrm{X}^{\omega} \\ \mathrm{Y}^{\omega} \end{bmatrix} \ . \tag{10}$$

The matrices A and B differ from the ones of the regular QRPA, as the last terms of equations (4) and (5) are zero because of charge conservation. The

resulting matrix elements are

$$\begin{aligned} A_{pn,p'n'}(J) &= (E_p + E_n)\delta_{pp'}\delta_{nn'} \\ &+g_{pp}(u_p u_n u_{p'} u_{n'} + v_p v_n v_{p'} v_{n'}) \langle p\, n\, ;\, J| \, V \, |p'\, n'\, ;\, J\rangle \\ &+g_{ph}(u_p v_n u_{p'} v_{n'} + v_p u_n v_{p'} u_{n'}) \langle p\, n^{-1}\, ;\, J| \, V_{RES} \, |p'\, n'^{-1}\, ;\, J\rangle \ , \end{aligned} \quad (11)$$

$$\begin{aligned} B_{pn,p'n'}(J) &= -g_{pp}(u_p u_n v_{p'} v_{n'} + v_p v_n u_{p'} u_{n'}) \langle p\, n\, ;\, J| \, V \, |p'\, n'\, ;\, J\rangle \\ &+g_{ph}(u_p v_n v_{p'} u_{n'} + v_p u_n u_{p'} v_{n'}) \langle p\, n^{-1}\, ;\, J| \, V_{RES} \, |p'\, n'^{-1}\, ;\, J\rangle \ , \end{aligned} \quad (12)$$

and the orthonormality and completeness relations take the form

$$\sum_{pn} \left(X_{pn}^{kJ^\pi *} X_{pn}^{k'J^\pi} - Y_{pn}^{kJ^\pi *} Y_{pn}^{k'J^\pi} \right) = \delta_{kk'} \ ,$$

$$\sum_{k} \left(X_{pn}^{kJ^\pi} X_{p'n'}^{kJ^\pi *} - Y_{pn}^{kJ^\pi} Y_{p'n'}^{kJ^\pi *} \right) = \delta_{pp'}\delta_{nn'} \ ,$$

$$\sum_{k} \left(X_{pn}^{kJ^\pi} Y_{p'n'}^{kJ^\pi *} - Y_{pn}^{kJ^\pi *} X_{p'n'}^{kJ^\pi} \right) = 0 \, .$$

2.3 Interaction parameters

Both the QRPA and pnQRPA have two important characteristic interaction parameters. These are the particle-hole and particle-particle interaction strengths, which appear in the particle-hole and particle-particle parts of the elements of matrices A and B (equations (4) and (5) in the QRPA, equations (11) and (12) in the pnQRPA). In the QRPA, these parameters are written as uppercase G_{ph} and G_{pp}, in the pnQRPA as lowercase g_{ph} and g_{pp}. This shall be the convention used in this work.

In QRPA, G_{pp} has little effect on the first excited states [13] and the common value of $G_{pp} = 1.00$ has been adapted for the examined nuclei. The first excited state of an even-even nucleus is most often a 2^+ state, which is of a particle-hole nature. Therefore, the value of G_{ph} has a significant effect on the energy of the first excited 2^+ state of the even-even nucleus. The value of G_{ph} was fixed for each nucleus separately by fitting the energy of the first 2^+ state to experimental data.

In pnQRPA, the particle-hole parameter g_{ph} has a large effect on the energy location of the Gamow-Teller giant resonance (GTGR). g_{pp} has more to do with the Gamow Teller beta decay transition amplitudes [14]. The value of g_{ph} was

fitted for each nucleus separately to approximately match the GTGR location to the empirical formula [1]:

$$\begin{aligned}\Delta E_{GT} &= \Delta E_C + \Delta E_{Z+1,N-1} \\ &= \left[1.444\left(Z+\frac{1}{2}\right)A^{-\frac{1}{3}} - 30.0(N-Z-2)A^{-1} + 5.57\right] \text{ MeV},\end{aligned} \tag{13}$$

where ΔE_c is the Coulomb energy and $\Delta E_{Z+1,N-1}$ is the energy difference between the GTGR state and the 0^+ isobaric analogue state of the odd-odd nucleus.

The particle-particle interaction parameter g_{pp} is often used to fit the $\log ft$ value of the transition from the first 1^+ state of the odd-odd nucleus to the ground state of the even-even nucleus [13, 15]. In this work, to better examine the systematics of Gamow-Teller beta decay, an array of constant values of g_{pp} = 0.6, 0.7, 0.8, 0.9 is assigned. By fitting the so called geometric means of the beta decay matrix elements, the behaviour of the axial-vector coupling constant g_A is expressed as a function of the mass number A for each value of g_{pp}. This gives rise to an opportunity to find a systematic behaviour of g_A for a given value of g_{pp}.

2.4 Single particle bases and pairing parameters

Ground-state to ground state beta decays were studied using a different method in the author's earlier work [16]. The single particle bases and pairing parameters used here are exactly the same and the following discussion from [16] is also valid for the present work.

Up to $A = 108$ a valence space consisting of 11 states, the entire 1p-0f-0g and 2s-1d-0h shells, was used. For $A = 110$ and onwards also the 2p and 1f shells were included and the valence space was expanded to 15 states. The valence spaces are visualized in Figure 3. The single particle bases are built by using a Coulomb-corrected Woods-Saxon potential and solving the radial Schrödinger equation [17]. The Woods-Saxon parameters used were the ones given by Bohr and Mottelson in [18]. The bases of ^{100}Mo, ^{100}Ru, ^{114}Pd and ^{114}Cd are given in Tables 1 and 2.

For the two-body part of the interactions, the renormalized Bonn-A G-matrix [9, 15] has been used and the neutron and proton pairing strength parameters A^p_{pair} and A^n_{pair} were fitted such that the lowest quasiparticle energies from the

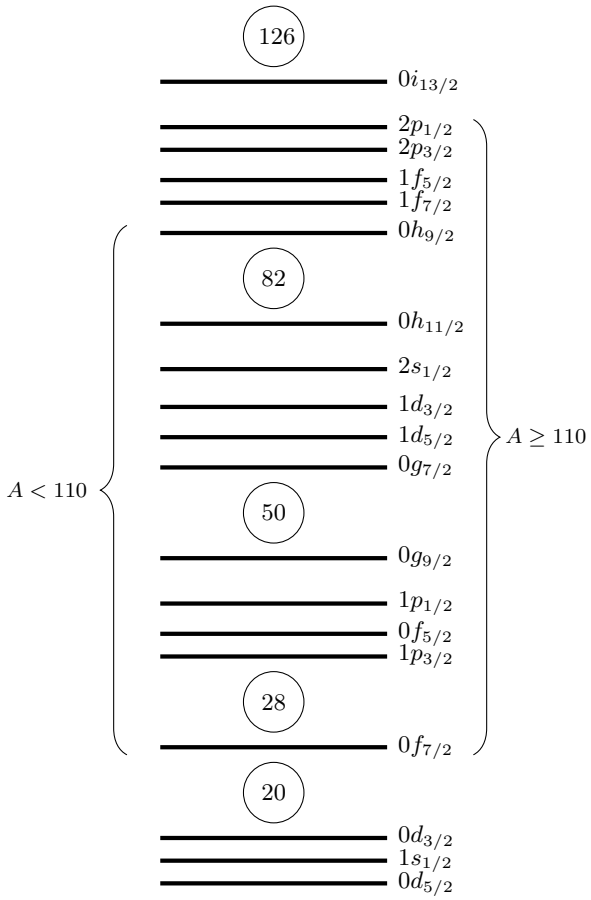

Figure 3: A schematic figure of the orbitals used to form the bases for nuclei with $A < 110$ and $A \geq 110$.

BCS calculation matches the pairing gaps:

$$E^p_{qp}(\text{lowest}) = \Delta_p, \quad \text{and } E^n_{qp}(\text{lowest}) = \Delta_n,$$

where the pairing gaps can be calculated by the three-point formula [19]

$$\Delta_p(A,Z) = \frac{1}{4}(-1)^{Z+1}\left[S_p(A+1,Z+1) - 2S_p(A,Z) + S_p(A-1,Z-1)\right],$$
$$\Delta_n(A,Z) = \frac{1}{4}(-1)^{A-Z+1}\left[S_n(A+1,Z) - 2S_n(A,Z) + S_n(A-1,Z)\right], \quad (14)$$

where S_i is the proton or neutron separation energy.

Table 1: The single particle bases of ^{100}Ru and ^{100}Mo for protons and neutrons respectively. The energies are in MeV.

nl_j (p)	$E_p(^{100}\text{Mo})$	$E_p(^{100}\text{Ru})$	nl_j(n)	$E_n(^{100}\text{Mo})$	$E_n(^{100}\text{Ru})$
$0f_{7/2}$	-16.067	-14.368	$0f_{7/2}$	-19.311	-20.422
$0f_{5/2}$	-11.537	-9.888	$0f_{5/2}$	-15.547	-16.590
$1p_{3/2}$	-11.203	-9.561	$1p_{3/2}$	-15.361	-16.394
$1p_{1/2}$	-9.473	-7.826	$1p_{1/2}$	-13.919	-14.917
$0g_{9/2}$	-8.311	-6.696	$0g_{9/2}$	-11.581	-12.623
$1d_{5/2}$	-2.811	-1.396	$1d_{5/2}$	-7.295	-8.195
$0g_{7/2}$	-1.474	0.121	$0g_{7/2}$	-5.913	-6.833
$2s_{1/2}$	-0.588	0.795	$2s_{1/2}$	-5.591	-6.386
$0h_{11/2}$	-0.106	1.414	$1d_{3/2}$	-4.814	-5.621
$1d_{3/2}$	0.202	1.601	$0h_{11/2}$	-3.501	-4.458
$0h_{9/2}$	9.102	10.400	$0h_{9/2}$	3.952	3.236

Table 2: The single particle bases of ^{114}Pd and ^{114}Cd for protons and neutrons respectively. The energies are in MeV.

nl_j (p)	$E_p(^{114}\text{Pd})$	$E_p(^{114}\text{Cd})$	nl_j(n)	$E_n(^{114}\text{Pd})$	$E_n(^{114}\text{Cd})$
$0f_{7/2}$	-18.224	-16.661	$0f_{7/2}$	-20.115	-21.105
$0f_{5/2}$	-14.180	-12.650	$0f_{5/2}$	-16.845	-17.785
$1p_{3/2}$	-13.413	-11.882	$1p_{3/2}$	-16.309	-17.238
$1p_{1/2}$	-11.835	-10.326	$1p_{1/2}$	-15.029	-15.933
$0g_{9/2}$	-10.845	-9.349	$0g_{9/2}$	-12.814	-13.748
$1d_{5/2}$	-5.255	-3.827	$1d_{5/2}$	-8.535	-9.361
$0g_{7/2}$	-4.647	-3.212	$0g_{7/2}$	-7.814	-8.659
$0h_{11/2}$	-2.970	-1.565	$2s_{1/2}$	-6.777	-7.524
$2s_{1/2}$	-2.759	-1.505	$1d_{3/2}$	-6.252	-7.010
$1d_{3/2}$	-2.313	-1.008	$0h_{11/2}$	-5.137	-6.004
$1f_{7/2}$	2.659	3.909	$1f_{7/2}$	-1.208	-1.864
$2p_{3/2}$	4.675	5.681	$2p_{3/2}$	-0.429	-0.835
$0h_{9/2}$	5.577	6.877	$2p_{1/2}$	0.082	-0.138
$2p_{1/2}$	5.894	6.875	$1f_{5/2}$	1.394	0.952
$1f_{5/2}$	6.616	7.681	$0h_{9/2}$	1.651	0.946

2.5 Allowed beta decay in the QRPA framework

With the QRPA and pnQRPA equations solved by, for example, numerical methods, one can obtain theoretical beta decay matrix elements describing beta decay or electron capture to or from states of the even-even reference nucleus [1]. In this work, the focus is set only on allowed Gamow-Teller beta decays, that is,

processes with an angular momentum change of $\Delta J = 1$ and no change in parity. The equations to calculate ground state to ground state decays are presented in this chapter as well as the means to calculate decays from an odd-odd nucleus to excited states of an even-even nucleus.

2.5.1 General theory of allowed beta decay

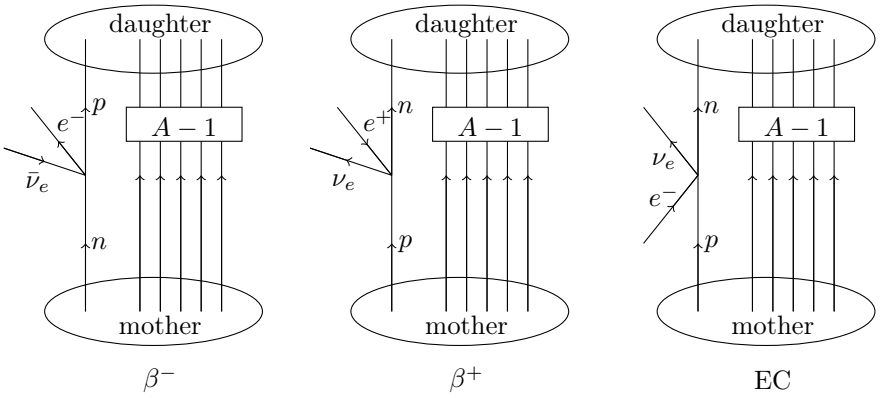

Figure 4: The Feynman diagrams of β^-, β^+ and EC decays in the impulse approximation: only one nucleon is considered to be affected by the weak decay process whereas the remaining $A-1$ nucleons remain unaffected [1].

In a single beta decay, there are always some resultant particles produced apart from the mother and daughter nuclei. The same holds true for an electron capture (EC) transition, except that an electron is captured instead of produced. The Feynman diagrams of these decay types are presented in Figure 4. The "extra" particles involved in the processes are the electron or the positron and the neutrino or the antineutrino depending on the type of the transition.

To be defined as "allowed", the change in the angular momentum in the transition from the mother to daughter nucleus must result only from the spins of the involved leptons [20]. For example, in a β^- decay the resultant electron and antineutrino cannot carry any orbital angular momentum. With each of the leptons involved having a spin of $s = \frac{1}{2}$, the change in angular momentum can only result from the spins being parallel $S = 1$ or antiparallel $S = 0$. As the leptons carry no orbital angular momentum, the parities of the initial and final states must also be identical. This leads to the selection rules for allowed β/EC decay [20]

$$\Delta J = 0,\, 1\,, \qquad \Delta\pi = \text{no}\,. \tag{15}$$

The transitions with no angular momentum change are called Fermi

decays [21] and those with $\Delta J = 1$ are called Gamow-Teller decays [22]. This work concentrates solely on Gamow-Teller transitions. The Fermi decay does not contribute to the beta transitions of interest in the thesis.

The half-life of a Gamow-Teller beta decay can be calculated from [1]

$$t_{1/2} = \frac{\kappa}{f_0 B_{GT}} \,, \tag{16}$$

where $\kappa = 6147\,\mathrm{s}$, f_0 is a phase space integral containing the lepton kinematics and B_{GT} is the reduced Gamow-Teller transition probability

$$B_{GT} = \frac{g_A^2}{2J_i + 1} \left| \mathcal{M}_{GT} \right|^2 \,. \tag{17}$$

The quantity $\mathcal{M}_{GT}$ is the Gamow-Teller transition amplitude described in the next subsections for different kinds of Gamow-Teller decays. These nuclear matrix elements can, in a general form, be written as [1]

$$\mathcal{M}_{GT} = (\xi_f \; J_f || \sigma || \xi_i \; J_i) = \sum_{ab} \mathcal{M}(ab) (\xi_f \; J_f || [c_a^\dagger \widetilde{c}_b]_1 || \xi_i \; J_i) \,, \tag{18}$$

where the operator σ is the Pauli spin operator and the reduced single particle matrix element reads

$$\mathcal{M}_{GT}(pn) = \sqrt{2} \delta_{n_p n_n} \delta_{l_p l_n} \widehat{j_p} \widehat{j_n} (-1)^{l_p + j_p + \frac{3}{2}} \begin{Bmatrix} \frac{1}{2} & \frac{1}{2} & 1 \\ j_n & j_p & l_p \end{Bmatrix} \,. \tag{19}$$

The regular particle creation and annihilation operators of equation (18) are related to the quasiparticle picture by the Bogoliubov-Valatin transformation [23, 24]:

$$\begin{aligned} a_\alpha^\dagger &= u_a c_\alpha^\dagger + v_a \widetilde{c}_\alpha \,, \\ \widetilde{a}_\alpha &= u_a \widetilde{c}_\alpha - v_a c_\alpha^\dagger \,. \end{aligned} \tag{20}$$

The common quantity, the "log ft" value, is taken as the basis of evaluating the theoretical calculations in this work. The log ft value is defined as [1]

$$\log ft = \log_{10}(f_0 t_{1/2}[s]) = \log_{10} \left(\frac{\kappa}{\frac{g_A}{2J_i+1} |\mathcal{M}_{GT}|^2} \right) \,. \tag{21}$$

The experimental log ft values of a vast number of nuclei are well measured making it a convenient tool in comparing theoretical calculations to experiment. Moreover, the log ft value depends on nuclear structure exclusively, which makes

it a good test for the competence of a theory.

2.5.2 Transitions to and from the even-even ground state

For the allowed Gamow-Teller beta transition amplitudes from the pnQRPA vacuum to a pnQRPA excited state, one has the form [1]:

$$\left(\omega||\beta^-_{GT}||QRPA\right) = \delta_{J1}\sqrt{3}\sum_{pn}\mathcal{M}_{GT}(pn)\left(u_p v_n X^\omega_{pn} + v_p u_n Y^\omega_{pn}\right) \ , \tag{22}$$

$$\left(\omega||\beta^+_{GT}||QRPA\right) = -\delta_{J1}\sqrt{3}\sum_{pn}\mathcal{M}_{GT}(pn)\left(v_p u_n X^\omega_{pn} + u_p v_n Y^\omega_{pn}\right) \ . \tag{23}$$

In equations (22) and (23) the reduced single-particle matrix element is as in equation (19)

The direction of the transition can be switched in equations (22) and (23) to make the Gamow-Teller transition amplitude from a pnQRPA excited state to the pnQRPA vacuum:

$$\left(QRPA||\beta^-_{GT}||\omega\right) = \delta_{J1}\sqrt{3}\sum_{pn}\mathcal{M}_{GT}(pn)\left(v_p u_n X^\omega_{pn} + u_p v_n Y^\omega_{pn}\right) \ , \tag{24}$$

$$\left(QRPA||\beta^+_{GT}||\omega\right) = -\delta_{J1}\sqrt{3}\sum_{pn}\mathcal{M}_{GT}(pn)\left(u_p v_n X^\omega_{pn} + v_p u_n Y^\omega_{pn}\right) \ . \tag{25}$$

2.5.3 Transitions between a QRPA and a pnQRPA state

Let the initial state be a pnQRPA state

$$|\omega_i\rangle = \sum_{p_i n_i}\left[X^\omega_{p_i n_i} A^\dagger_{p_i n_i}(J_i M_i) - Y^\omega_{p_i n_i}\widetilde{A}_{p_i n_i}(J_i M_i)\right]|QRPA\rangle \ ,$$

and the final state a QRPA one-phonon state

$$|\omega_f\rangle = \sum_{a_f \le b_f}\left[X^\omega_{a_f b_f} A^\dagger_{a_f b_f}(J_f M_f) - Y^\omega_{a_f b_f}\widetilde{A}_{a_f b_f}(J_f M_f)\right]|QRPA\rangle \ .$$

For Gamow-Teller transitions from a pnQRPA state to a QRPA state, one can

derive a result for the reduced transition amplitude [1]:

$$\begin{aligned}\left(\omega_f||\beta^{\mp}_{GT}||\omega_i\right) = &\sum_{\substack{p_i n_i \\ p_f \le p'_f}} \left[X^{\omega_f *}_{p_f p'_f} X^{\omega_i}_{p_i n_i} \mathcal{M}^{(\mp)}_{GT}\left(p_i\, n_i\,;\, J_i \,\rightarrow\, p_f\, p'_f\,;\, J_f\right)\right. \\ &\left. - Y^{\omega_f *}_{p_f p'_f} Y^{\omega_i}_{p_i n_i} \mathcal{M}^{(\pm)}_{GT}\left(p_i\, n_i\,;\, J_i \,\rightarrow\, p_f\, p'_f\,;\, J_f\right)\right] \\ &+ \sum_{\substack{p_i n_i \\ n_f \le n'_f}} \left[X^{\omega_f *}_{n_f n'_f} X^{\omega_i}_{p_i n_i} \mathcal{M}^{(\mp)}_{GT}\left(p_i\, n_i\,;\, J_i \,\rightarrow\, n_f\, n'_f\,;\, J_f\right)\right. \\ &\left. - Y^{\omega_f *}_{n_f n'_f} Y^{\omega_i}_{p_i n_i} \mathcal{M}^{(\pm)}_{GT}\left(p_i\, n_i\,;\, J_i \,\rightarrow\, n_f\, n'_f\,;\, J_f\right)\right]. \end{aligned} \tag{26}$$

The two-quasiparticle transition amplitudes of equation (26) are expressed as

$$\begin{aligned}&\mathcal{M}^{(\mp)}_{GT}\left(p_i\, n_i\,;\, J_i \,\rightarrow\, p_f\, p'_f\,;\, J_f\right) = \sqrt{3}\widehat{J}_i\widehat{J_f}\mathcal{N}_{p_f p'_f}(J_f) \\ &\times\left[\delta_{p_i p'_f}(-1)^{j_{p_f}+j_{n_i}+1}\begin{Bmatrix} J_i & J_f & 1 \\ j_{p_f} & j_{n_i} & j_{p'_f}\end{Bmatrix}\mathcal{B}^{(\mp)}_{GT}(p_f n_i)\mathcal{M}_{GT}(p_f n_i)\right. \\ &\left.+\delta_{p_i p_f}(-1)^{j_{p_f}+j_{n_i}+J_f+1}\begin{Bmatrix} J_i & J_f & 1 \\ j_{p'_f} & j_{n_i} & j_{p_f}\end{Bmatrix}\mathcal{B}^{(\mp)}_{GT}(p'_f n_i)\mathcal{M}_{GT}(p'_f n_i)\right],\end{aligned}$$

$$\begin{aligned}&\mathcal{M}^{(\pm)}_{GT}\left(p_i\, n_i\,;\, J_i \,\rightarrow\, n_f\, n'_f\,;\, J_f\right) = \sqrt{3}\widehat{J}_i\widehat{J_f}\mathcal{N}_{n_f n'_f}(J_f) \\ &\times\left[\delta_{n_i n'_f}(-1)^{j_{p_i}+j_{n_i}+J_i+1}\begin{Bmatrix} J_i & J_f & 1 \\ j_{n_f} & j_{p_i} & j_{n_i}\end{Bmatrix}\mathcal{B}^{(\mp)}_{GT}(p_i n_f)\mathcal{M}_{GT}(p_i n_f)\right. \\ &\left.+\delta_{n_i n_f}(-1)^{j_{p_i}+j_{n'_f}+J_i+J_f+1}\begin{Bmatrix} J_i & J_f & 1 \\ j_{n'_f} & j_{p_i} & j_{n_f}\end{Bmatrix}\mathcal{B}^{(\mp)}_{GT}(p_i n'_f)\mathcal{M}_{GT}(p_i n'_f)\right],\end{aligned}$$

where $\mathcal{B}^{\mp}_{GT}$ contains the occupation factors

$$\begin{aligned}\mathcal{B}^{(-)}_{GT}(if) &= u_i u_f \qquad \text{particle type} \\ \mathcal{B}^{(+)}_{GT}(if) &= v_i v_f \qquad \text{hole type}\,,\end{aligned}$$

and the single particle matrix elements $\mathcal{M}_{GT}(if)$ are as in equation (19).

Should the final state be a two-quadrupole-phonon state of equation (8), then

the reduced transition amplitude for a beta minus transition takes the form [13]

$$\begin{aligned}\mathcal{M}^{GT(-)}_{J_F,1}(u,v) &= (J^+_f||\beta^-_{GT}||1^+) \\ &= -40\frac{1}{\sqrt{2}}\sqrt{3(2J_f+1)} \\ &\times \sum_{pnp'n'} \mathcal{M}(pn)\Big[u_p v_n X_{pp'}(2^+,\,1)X_{nn'}(2^+,\,1)X_{p'n'}(1^+,\,1) \\ &+ v_p u_n Y_{pp'}(2^+,\,1)Y_{nn'}(2^+,\,1)Y_{p'n'}(1^+,\,1)\Big] \begin{Bmatrix} j_p & j_{p'} & 2 \\ j_n & j_{n'} & 2 \\ 1 & 1 & J_f \end{Bmatrix} . \end{aligned} \tag{27}$$

The corresponding beta plus or EC amplitude follows from equation (27) by

$$\mathcal{M}^{GT(+)}_{J_F J_i}(u,v) = (J^+_f||\beta^+_{GT}||1^+) = -\mathcal{M}^{GT(-)}_{J_F J_i}(v,u)\,. \tag{28}$$

It should be noted that in (27) the amplitudes $X_{aa'}$ and $Y_{aa'}$ differ from the X and Y amplitudes of (2) as discussed in [13].

3 Calculations and discussion

To test the formalism of Section 2 and to gain insights on the behaviour of the effective value of the axial-vector coupling constant g_A, a series of QRPA calculations is performed systematically through the mass region $A = 100-134$. The beta decay properties of ground state to ground state decays are analyzed first through the concept of a geometric mean of the left and right Gamow-Teller matrix elements. Through this examination, a linear g_A model is proposed and the ground state to ground state decay $\log ft$ values are calculated within this model using a reasonably average value of $g_{pp} = 0.7$.

The linear g_A model is then tested further and the analysis is extended to decays to the first excited 2^+ states and the 0^+ and 2^+ collective quadrupole two-phonon states of the even-even nuclei. Theoretical predictions of $\log ft$ values are made for every process with experimental data available.

3.1 Ground state to ground state decays and the linear g_A model

One possible way to examine the beta decay matrix elements is by taking the geometric mean $\mathcal{M}^m_{GT}$ of the left and right matrix elements $\mathcal{M}^l_{GT}$ and $\mathcal{M}^r_{GT}$. This geometric mean seems to be only weakly dependent on the value of g_{pp} [25] and thus allows a very sophisticated approach to studying the overall behaviour of g_A. One can calculate the experimental geometric means of the NMEs (multiplied by g_A) from

$$\begin{aligned} g_A\mathcal{M}^m_{GT}(exp.) &= g_A\sqrt{|\mathcal{M}^l_{GT}(exp.)\mathcal{M}^r_{GT}(exp.)|} \\ &= \sqrt{\kappa\sqrt{\frac{(2J^l_i+1)(J^r_i+1)}{10^{\log ft_l(exp.)}\times 10^{\log ft_r(exp.)}}}}\,. \end{aligned} \tag{29}$$

This quantity is actually independent of the value of g_A taken for theoretical calculations, which permits g_A to be left as a free parameter to fit calculations to experimental data. The geometric mean is taken as a base of analysis in this work. The calculated experimental geometric means for the investigated mass region are presented in Table 3.

Table 3: Experimental geometric means of the NMEs. The experimental log ft values are extracted from [12], except [1)] is extrapolated from systematics of similar neighbouring decays and [2)] is from [26]

		Process			$\log ft_{exp}$				
A	Z	Z	Z+1	Z + 2	left	right	$g_A M_{GT}(l)$	$g_A M_{GT}(r)$	$g_A M^m_{GT}$
100	40	$Zr(0^+)$	$\rightarrow Nb(1^+) \rightarrow$	$Mo(0^+)$	4.65	5.1	0.371	0.382	0.377
100	42	$Mo(0^+)$	$\leftarrow Tc(1^+) \rightarrow$	$Ru(0^+)$	4.4	4.59	0.857	0.688	0.768
102	42	$Mo(0^+)$	$\rightarrow Tc(1^+) \rightarrow$	$Ru(0^+)$	4.21	4.778	0.616	0.554	0.584
104	44	$Ru(0^+)$	$\leftarrow Rh(1^+) \rightarrow$	$Pd(0^+)$	4.32	4.55	0.939	0.721	0.823
106	44	$Ru(0^+)$	$\rightarrow Rh(1^+) \rightarrow$	$Pd(0^+)$	4.31	5.168	0.548	0.354	0.441
106	46	$Pd(0^+)$	$\leftarrow Ag(1^+) \rightarrow$	$Cd(0^+)$	4.92	$4.4^{1)}$	0.471	0.857	0.635
108	44	$Ru(0^+)$	$\rightarrow Rh(1^+) \rightarrow$	$Pd(0^+)$	$4.2^{2)}$	5.5	0.623	0.241	0.388
108	46	$Pd(0^+)$	$\leftarrow Ag(1^+) \rightarrow$	$Cd(0^+)$	4.70	4.425	0.607	0.833	0.711
110	46	$Pd(0^+)$	$\leftarrow Ag(1^+) \rightarrow$	$Cd(0^+)$	4.09	4.6596	1.224	0.635	0.882
112	48	$Cd(0^+)$	$\leftarrow In(1^+) \rightarrow$	$Sn(0^+)$	4.70	4.12	0.607	1.183	0.847
114	46	$Pd(0^+)$	$\rightarrow Ag(1^+) \rightarrow$	$Cd(0^+)$	4.199	5.1	0.623	0.383	0.488
114	48	$Cd(0^+)$	$\leftarrow In(1^+) \rightarrow$	$Sn(0^+)$	4.89	4.4701	0.487	0.790	0.621
116	48	$Cd(0^+)$	$\leftarrow In(1^+) \rightarrow$	$Sn(0^+)$	4.47	4.662	0.790	0.634	0.708
118	48	$Cd(0^+)$	$\rightarrow In(1^+) \rightarrow$	$Sn(0^+)$	3.91	4.79	0.870	0.547	0.690
118	50	$Sn(0^+)$	$\leftarrow Sb(1^+) \leftarrow$	$Te(0^+)$	4.525	5.0	0.742	0.248	0.429
120	48	$Cd(0^+)$	$\rightarrow In(1^+) \rightarrow$	$Sn(0^+)$	4.1	5.023	0.699	0.418	0.541
122	48	$Cd(0^+)$	$\rightarrow In(1^+) \rightarrow$	$Sn(0^+)$	3.95	5.11	0.830	0.378	0.561
122	52	$Te(0^+)$	$\leftarrow I(1^+) \leftarrow$	$Xe(0^+)$	4.95	5.191	0.455	0.199	0.301
124	54	$Xe(0^+)$	$\leftarrow Cs(1^+) \leftarrow$	$Ba(0^+)$	5.10	5.2	0.383	0.197	0.275
126	54	$Xe(0^+)$	$\leftarrow Cs(1^+) \leftarrow$	$Ba(0^+)$	5.066	5.36	0.398	0.164	0.255
128	52	$Te(0^+)$	$\leftarrow I(1^+) \rightarrow$	$Xe(0^+)$	5.049	6.061	0.406	0.127	0.227
128	54	$Xe(0^+)$	$\leftarrow Cs(1^+) \leftarrow$	$Ba(0^+)$	4.847	5.28	0.512	0.180	0.303
130	54	$Xe(0^+)$	$\leftarrow Cs(1^+) \rightarrow$	$Ba(0^+)$	5.073	5.36	0.395	0.284	0.335
134	56	$Ba(0^+)$	$\leftarrow La(1^+) \leftarrow$	$Ce(0^+)$	4.883	5.23	0.491	0.190	0.306

The formalism of Section 2 was first used to examine the ground state to ground state decays in the investigated mass region. Four rounds of pnQRPA calculations were performed using typical values of $g_{pp} = 0.6,\ 0.7,\ 0.8,\ 0.9$ in order to analyze the left and right branches of Gamow-Teller beta decay from each odd-odd nucleus. With these values one does not have to worry about the breaking

of the pnQRPA as $g_{pp} \leq 1$ has been deemed safe over this mass region in [16]. From the solved wave functions of the first 1^+ states of the odd-odd nuclei, the transition amplitudes were calculated using equations (24) and (25). Theoretical geometric means of these matrix elements were then calculated for each g_{pp} and fitted to the experimental values by altering the value of g_A. The calculated matrix elements and geometric means for $g_{pp} = 0.7$ are given in Table 4 and visualized in Figure 5. Resulting values of g_A for each value of g_{pp} are presented in Figure 6 as a function of the mass number A.

In Figure 5 one can see a decreasing behaviour of the NMEs as a function of A. At first, around $A = 100 - 112$ there is some alternation between the left and right matrix elements being larger than the other, but at $A = 112$ onwards the right matrix elements are always smaller than the left ones and eventually become only about a fifth of the magnitude of the left matrix elements. The experimental log ft values in the left branch are generally smaller than the log ft values in the right branch so this is in good agreement with experimentally observed behaviour.

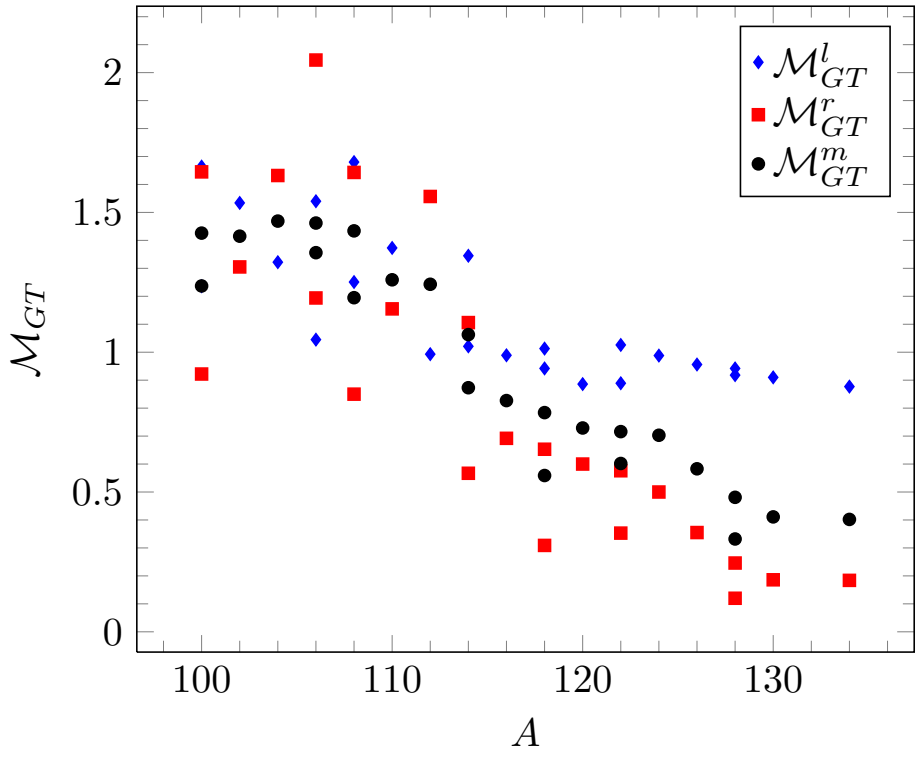

Figure 5: Theoretical beta decay matrix elements as a function of the mass number A. The computations were done with $g_{pp} = 0.7$. The effect of g_A has not yet been taken into account.

Table 4: Theoretical geometric means of the NMEs with $g_{pp} = 0.7$. The values of g_A were fixed for each process by fitting the theoretical geometric mean to the experimental value.

		Process						$g_A M^m_{GT}$	
A	Z	Z	Z+1	Z + 2	g_A	$M^{\text{th.}}_{GT}(l)$	$M^{\text{th.}}_{GT}(r)$	exp.	th.
100	40	$Zr(0^+)$	$\rightarrow Nb(1^+) \rightarrow$	$Mo(0^+)$	0.30	1.664	0.922	0.377	0.372
100	42	$Mo(0^+)$	$\leftarrow Tc(1^+) \rightarrow$	$Ru(0^+)$	0.54	1.236	1.645	0.768	0.770
102	42	$Mo(0^+)$	$\rightarrow Tc(1^+) \rightarrow$	$Ru(0^+)$	0.41	1.534	1.305	0.584	0.580
104	44	$Ru(0^+)$	$\leftarrow Rh(1^+) \rightarrow$	$Pd(0^+)$	0.56	1.322	1.632	0.823	0.823
106	44	$Ru(0^+)$	$\rightarrow Rh(1^+) \rightarrow$	$Pd(0^+)$	0.33	1.540	1.194	0.441	0.447
106	46	$Pd(0^+)$	$\leftarrow Ag(1^+) \rightarrow$	$Cd(0^+)$	0.43	1.045	2.045	0.635	0.629
108	44	$Ru(0^+)$	$\rightarrow Rh(1^+) \rightarrow$	$Pd(0^+)$	0.32	1.680	0.8502	0.388	0.382
108	46	$Pd(0^+)$	$\leftarrow Ag(1^+) \rightarrow$	$Cd(0^+)$	0.50	1.251	1.643	0.711	0.717
110	46	$Pd(0^+)$	$\leftarrow Ag(1^+) \rightarrow$	$Cd(0^+)$	0.70	1.373	1.155	0.882	0.882
112	48	$Cd(0^+)$	$\leftarrow In(1^+) \rightarrow$	$Sn(0^+)$	0.68	0.993	1.557	0.847	0.846
114	46	$Pd(0^+)$	$\rightarrow Ag(1^+) \rightarrow$	$Cd(0^+)$	0.56	1.345	0.5676	0.488	0.489
114	48	$Cd(0^+)$	$\leftarrow In(1^+) \rightarrow$	$Sn(0^+)$	0.58	1.021	1.106	0.621	0.616
116	48	$Cd(0^+)$	$\leftarrow In(1^+) \rightarrow$	$Sn(0^+)$	0.86	0.989	0.692	0.708	0.711
118	48	$Cd(0^+)$	$\rightarrow In(1^+) \rightarrow$	$Sn(0^+)$	0.88	0.942	0.653	0.690	0.690
118	50	$Sn(0^+)$	$\leftarrow Sb(1^+) \leftarrow$	$Te(0^+)$	0.77	1.013	0.309	0.429	0.430
120	48	$Cd(0^+)$	$\rightarrow In(1^+) \rightarrow$	$Sn(0^+)$	0.74	0.886	0.600	0.541	0.540
122	48	$Cd(0^+)$	$\rightarrow In(1^+) \rightarrow$	$Sn(0^+)$	0.78	0.889	0.576	0.561	0.558
122	52	$Te(0^+)$	$\leftarrow I(1^+) \leftarrow$	$Xe(0^+)$	0.50	1.026	0.353	0.301	0.301
124	54	$Xe(0^+)$	$\leftarrow Cs(1^+) \leftarrow$	$Ba(0^+)$	0.39	0.988	0.500	0.275	0.274
126	54	$Xe(0^+)$	$\leftarrow Cs(1^+) \leftarrow$	$Ba(0^+)$	0.44	0.956	0.355	0.255	0.256
128	52	$Te(0^+)$	$\leftarrow I(1^+) \rightarrow$	$Xe(0^+)$	0.68	0.918	0.120	0.227	0.226
128	54	$Xe(0^+)$	$\leftarrow Cs(1^+) \leftarrow$	$Ba(0^+)$	0.63	0.942	0.246	0.303	0.304
130	54	$Xe(0^+)$	$\leftarrow Cs(1^+) \rightarrow$	$Ba(0^+)$	0.81	0.910	0.186	0.335	0.333
134	56	$Ba(0^+)$	$\leftarrow La(1^+) \leftarrow$	$Ce(0^+)$	0.76	0.877	0.184	0.306	0.305

In figure 6 one can immediately see that, with respect to increase in g_{pp}, g_A becomes more unstable with increasing A. The value of $g_{pp} = 0.9$ is thus discarded as only a small variation in g_A is desired. It is also evident, given a reasonable interval of g_{pp} values, that the geometric mean does not depend very much on the value of g_{pp} as expected. This can be seen in Figure 6 as the data

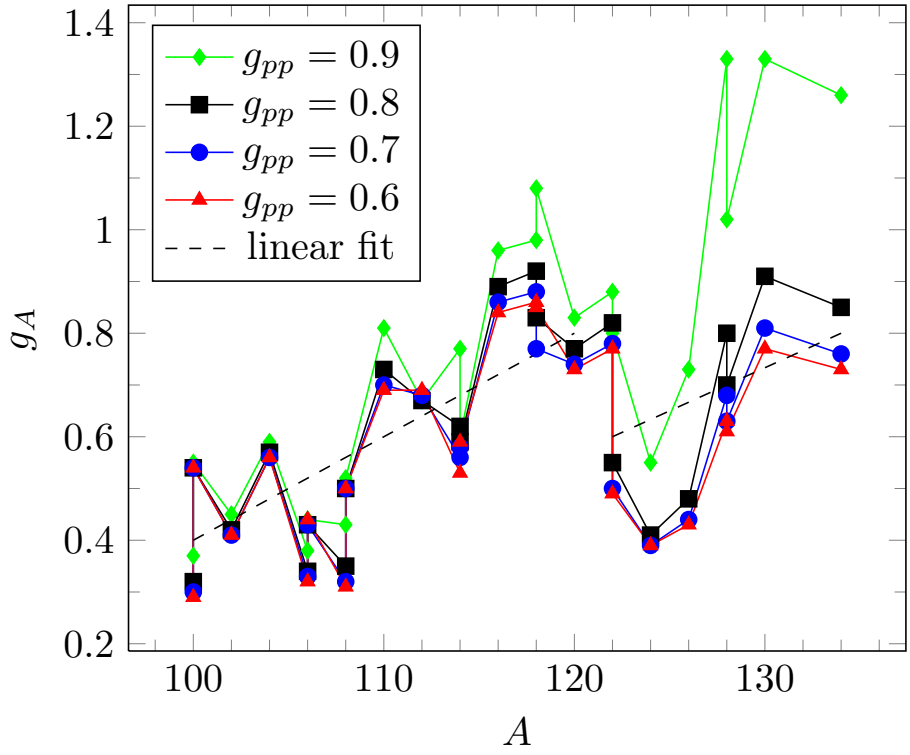

Figure 6: Values of g_A as a function of the mass number A. The data points were produced by fitting the theoretical geometric means to the experimental values of Table 3.

points representing different values of g_{pp} for separate nuclei are very tightly packed close to each other. In other words, it does not take a significant change in g_A to compensate for a relatively large change in g_{pp}.

Interestingly enough, the calculations replicate the experimental geometric means of the NMEs for $g_{pp} = 0.6,\ 0.7,\ 0.8$ only for values of $g_A < 1$. This is solid evidence that an effective g_A is needed when working with this mass region. Not only are the values in general smaller than the bare value of $g_A = 1.25$ but in some cases an effective value as low as $g_A = 0.3$ is required.

The zigzag behaviour of Figure 6 might rise from the filling of orbitals in the simple shell model. At $A = 100,\ 108,\ 122$ there are two different possible beta decay processes which result in notably different effective values of g_A. The process giving the smaller g_A in these three cases appears to include a nucleus with all proton or neutron orbitals filled. However, in the $A = 106$ processes the order is reversed. In the $A = 100$ and $A = 122$ processes both of the even-even nuclei involved have their protons or neutrons at full orbitals in the process

yielding the smaller g_A. This could explain the large difference in g_A within a single mass number.

Decays to or from a nucleus with full proton or neutron orbitals results a higher transition amplitude than the neighbouring processes between the isotopes of the same element. For example, in the β^- decay of ^{106}Pd to ^{106}Cd the neutron number of the Cd nucleus is 58, closing the $0g_{7/2}$ shell. This results to a large right matrix element of $\mathcal{M}^{th}_{GT}(r) = 2.045$, much larger than of the Pd to Cd process at $A = 108$ with $\mathcal{M}^{th}_{GT}(r) = 1.680$ or at $A = 110$ with $\mathcal{M}^{th}_{GT}(r) = 1.155$. There seems to be something in the involved systematics which gives more strength to decays to or from a nucleus with closed shells. How the filling of orbitals affects the g_A behaviour of Figure 6 is difficult to say as nearly every examined triplet involves one nucleus with a filled neutron orbital. The average effect appears to be quite random.

In Figure 6 one can see an interesting rising behaviour in g_A as a function of A. There seem to be two mass regions in which g_A behaves, on average, linearly with a positive slope. By making an approximation of the equations of the two lines and combining them, a function governing the entire mass range $A = 100 - 134$ can be constructed. The function constructed along the dashed lines of Figure 6 reads as

$$g_A = \begin{cases} 0.02A - 1.6, & \text{for} A \in [100,\ 120] \\ \frac{1}{60}A - \frac{43}{30}, & \text{for} A \in [122,\ 134] \end{cases} . \tag{30}$$

By using this function to generate values of g_A and adopting a reasonably average value of $g_{pp} = 0.7$, the Gamow-Teller matrix elements were calculated for ground state to ground state decays. The resulting left and right $\log ft$ values are presented in Table 5. The agreement with experiment is decent at the very least. The decays which are not quite along the line of equation (30) in Figure 6 expectedly produce somewhat less accurate predictions, for example the $A = 124$ triplet. The use of this linear g_A is still feasible as the overall accuracy of the predictions is very good for such a simple model.

Table 5: Calculated $\log ft$ values for ground state to ground state decays compared with experiment. The computations were performed with a linear g_A obtained from equation (30) and $g_{pp} = 0.7$. The experimental data is extracted from [12], except [1)] is extrapolated from systematics of similar neighbouring decays and [2)] from [26].

		Process				$\log ft_{exp}$		$\log ft_{th}$	
A	Z	Z	Z+1	Z + 2	g_A	left	right	left	right
100	40	$Zr(0^+)$	$\rightarrow Nb(1^+) \rightarrow$	$Mo(0^+)$	0.40	4.65	5.1	4.14	5.13
100	42	$Mo(0^+)$	$\leftarrow Tc(1^+) \rightarrow$	$Ru(0^+)$	0.40	4.4	4.59	4.88	4.63
102	42	$Mo(0^+)$	$\rightarrow Tc(1^+) \rightarrow$	$Ru(0^+)$	0.44	4.21	4.778	4.13	4.75
104	44	$Ru(0^+)$	$\leftarrow Rh(1^+) \rightarrow$	$Pd(0^+)$	0.48	4.32	4.55	4.66	4.48
106	44	$Ru(0^+)$	$\rightarrow Rh(1^+) \rightarrow$	$Pd(0^+)$	0.52	4.31	5.168	3.98	4.68
106	46	$Pd(0^+)$	$\leftarrow Ag(1^+) \rightarrow$	$Cd(0^+)$	0.52	4.92	4.4[1)]	4.80	4.21
108	44	$Ru(0^+)$	$\rightarrow Rh(1^+) \rightarrow$	$Pd(0^+)$	0.56	4.2[2)]	5.5	3.84	4.91
108	46	$Pd(0^+)$	$\leftarrow Ag(1^+) \rightarrow$	$Cd(0^+)$	0.56	4.70	4.425	4.57	4.34
110	46	$Pd(0^+)$	$\leftarrow Ag(1^+) \rightarrow$	$Cd(0^+)$	0.60	4.09	4.6596	4.43	4.58
112	48	$Cd(0^+)$	$\leftarrow In(1^+) \rightarrow$	$Sn(0^+)$	0.64	4.70	4.12	4.67	4.27
114	46	$Pd(0^+)$	$\rightarrow Ag(1^+) \rightarrow$	$Cd(0^+)$	0.68	4.119	5.1	3.87	5.09
114	48	$Cd(0^+)$	$\leftarrow In(1^+) \rightarrow$	$Sn(0^+)$	0.68	4.89	4.4701	4.58	4.51
116	48	$Cd(0^+)$	$\leftarrow In(1^+) \rightarrow$	$Sn(0^+)$	0.72	4.47	4.662	4.56	4.87
118	48	$Cd(0^+)$	$\rightarrow In(1^+) \rightarrow$	$Sn(0^+)$	0.76	3.91	4.79	4.08	4.87
118	50	$Sn(0^+)$	$\leftarrow Sb(1^+) \leftarrow$	$Te(0^+)$	0.76	4.525	5.0	4.49	5.05
120	48	$Cd(0^+)$	$\rightarrow In(1^+) \rightarrow$	$Sn(0^+)$	0.80	4.1	5.023	4.08	4.90
122	48	$Cd(0^+)$	$\rightarrow In(1^+) \rightarrow$	$Sn(0^+)$	0.60	3.95	5.11	4.33	5.19
122	52	$Te(0^+)$	$\leftarrow I(1^+) \leftarrow$	$Xe(0^+)$	0.60	4.95	5.191	4.69	5.12
124	54	$Xe(0^+)$	$\leftarrow Cs(1^+) \leftarrow$	$Ba(0^+)$	0.63	5.10	5.2	4.68	4.79
126	54	$Xe(0^+)$	$\leftarrow Cs(1^+) \leftarrow$	$Ba(0^+)$	0.67	5.066	5.36	4.65	5.04
128	52	$Te(0^+)$	$\leftarrow I(1^+) \rightarrow$	$Xe(0^+)$	0.70	5.049	6.061	4.65	6.42
128	54	$Xe(0^+)$	$\leftarrow Cs(1^+) \leftarrow$	$Ba(0^+)$	0.70	4.847	5.28	4.63	5.32
130	54	$Xe(0^+)$	$\leftarrow Cs(1^+) \rightarrow$	$Ba(0^+)$	0.73	5.073	5.36	4.62	6.00
134	56	$Ba(0^+)$	$\leftarrow La(1^+) \leftarrow$	$Ce(0^+)$	0.80	4.883	5.23	4.57	5.45

The semi-magic isotopes of Sn have, in earlier work, brought some trouble in calculating the ground state to ground state decays with constant g_A values [16]. The BCS quasiparticle theory does not function well at closed shells and some problems are often expected in these calculations. However, every process

involving a tin isotope is actually predicted very well by the linear g_A model.

The accuracy of the predictions of Table 5 were evaluated by taking the mean deviation from the experimental $\log ft$ values. The mean deviation is calculated from

$$\Delta_m = \frac{1}{\#D} \sum_D |\log ft_{th} - \log ft_{exp}| \,, \tag{31}$$

where the summation is over all of the investigated processes. The calculated mean deviations result to $\Delta_m = 0.27, 0.18, 0.23$ for the left branch, right branch and all decays respectively. The mean deviation from experiment is rather small overall, even smaller if examining only the right branch of decays. Thus, the predictions given by the linear g_A model can be deemed reliable for ground state to ground state decays.

One might be able to enhance some of the results of Table 5 by altering the value of g_{pp} for different mass numbers. However, the comfortability of using a constant value would be lost. Moreover, the larger deviations often happen in processes where both the left and right theoretical $\log ft$ values are too small. In these situations, only the left or the right branch could be fit to experimental data by g_{pp}, but never both. These processes are easily recognized to be deviations from the linear model of g_A instead.

3.2 Decays to excited states

The examination of the linear g_A model was then expanded to decays from the 1^+ ground state of the odd-odd nuclei to the first excited 2^+ state of the even-even nuclei and to the 0^+ and 2^+ two-phonon states constructed from the wave function of the first 2^+ state. The wave function of the first 2^+ state was computed by the QRPA formalism and the required transition amplitudes were determined by using the equations in Section 2.5.3.

All processes in the investigated mass region with experimental data available for decays to these excited states have been included and the results of the calculations are presented in Table 6 and visualized in Figures 7, 8 and 9. The predictions of $\log ft$ values for decays beyond ground states are generally more tricky. The QRPA and pnQRPA calculations are often accurate for only the lowest-lying states and even then the wave function of the obtained state might connect to some other state with the same angular momentum and parity, perhaps at a higher energy.

Still, the accuracy of the prediction is quite passable, especially for decays to the first 2^+ state, the energy of which was fitted to an experimental value. The calculated $\log ft$ values for decays to the two-phonon 2^+ state are systematically too large compared to the experimental values. For these states there seems to be some mechanism that the present formalism does not account for. The computed $\log ft$ values of Table 6 result to mean deviations of 0.47 (with the badly functioning Rh to Pd processes omitted) for decays to the 2_1^+ state, 0.74 to the 0_{2-ph}^+ state and 0.82 to the 2_{2-ph}^+ state.

Table 6: Calculated $\log ft$ values for decays to excited states compared with experiment. The computations were performed with a linear g_A obtained from equation (30) and $g_{pp} = 0.7$. The experimental data is extracted from [12].

A	Process			E_f (MeV)	g_A	$\log ft_{exp}$	$\log ft_{th}$
100	$\mathrm{Nb}(1_{gs}^+)$	$\rightarrow$ β^-	$\mathrm{Mo}(2_1^+)$	0.5356	0.40	5.65	5.94
	$\mathrm{Nb}(1_{gs}^+)$	$\rightarrow$ β^-	$\mathrm{Mo}(0_2^+)$	0.6951	0.40	5.7	5.72
	$\mathrm{Nb}(1_{gs}^+)$	$\rightarrow$ β^-	$\mathrm{Mo}(2_2^+)$	1.0638	0.40	5.9	6.76
100	$\mathrm{Tc}(1_{gs}^+)$	$\rightarrow$ β^-	$\mathrm{Ru}(2_1^+)$	0.5395	0.40	6.4	5.88
	$\mathrm{Tc}(1_{gs}^+)$	$\rightarrow$ β^-	$\mathrm{Ru}(0_2^+)$	1.1303	0.40	5.04	6.06
	$\mathrm{Tc}(1_{gs}^+)$	$\rightarrow$ β^-	$\mathrm{Ru}(2_2^+)$	1.3622	0.40	7.1	7.35
102	$\mathrm{Tc}(1_{gs}^+)$	$\rightarrow$ β^-	$\mathrm{Ru}(2_1^+)$	0.4751	0.44	5.99	6.24
	$\mathrm{Tc}(1_{gs}^+)$	$\rightarrow$ β^-	$\mathrm{Ru}(0_2^+)$	0.9437	0.44	6.60	5.60
	$\mathrm{Tc}(1_{gs}^+)$	$\rightarrow$ β^-	$\mathrm{Ru}(2_2^+)$	1.1030	0.44	≈ 7.0	6.80
104	$\mathrm{Rh}(1_{gs}^+)$	$\rightarrow$ β^+/EC	$\mathrm{Ru}(2_1^+)$	0.3580	0.48	5.42	5.94
	$\mathrm{Rh}(1_{gs}^+)$	$\rightarrow$ β^+/EC	$\mathrm{Ru}(0_2^+)$	0.9883	0.48	5.15	5.23

Continued on next page

Table 6 – *Continued from previous page*

A	Process			E_f (MeV)	g_A	$\log ft_{exp}$	$\log ft_{th}$
104	$Rh(1^+_{gs})$	$\rightarrow$ β^+/EC	$Ru(2^+_2)$	0.8931	0.48	—	6.05
104	$Rh(1^+_{gs})$	$\rightarrow$ β^-	$Pd(2^+_1)$	0.5558	0.48	5.80	7.43
	$Rh(1^+_{gs})$	$\rightarrow$ β^-	$Pd(0^+_2)$	1.3336	0.48	7.36	5.70
	$Rh(1^+_{gs})$	$\rightarrow$ β^-	$Pd(2^+_2)$	1.3417	0.48	8.7	7.13
106	$Rh(1^+_{gs})$	$\rightarrow$ β^-	$Pd(2^+_1)$	0.5119	0.52	5.865	9.07
	$Rh(1^+_{gs})$	$\rightarrow$ β^-	$Pd(0^+_2)$	1.1338	0.52	5.345	5.39
	$Rh(1^+_{gs})$	$\rightarrow$ β^-	$Pd(2^+_2)$	1.1280	0.52	6.55	6.70
106	$Ag(1^+_{gs})$	$\rightarrow$ β^+/EC	$Pd(2^+_1)$	0.5119	0.52	5.24	5.74
	$Ag(1^+_{gs})$	$\rightarrow$ β^+/EC	$Pd(0^+_2)$	1.1338	0.52	6.5	5.17
	$Ag(1^+_{gs})$	$\rightarrow$ β^+/EC	$Pd(2^+_2)$	1.1280	0.52	—	6.01
108	$Rh(1^+_{gs})$	$\rightarrow$ β^-	$Pd(2^+_1)$	0.4339	0.56	5.7	9.40
	$Rh(1^+_{gs})$	$\rightarrow$ β^-	$Pd(0^+_2)$	1.0528	0.56	5.6	5.15
	$Rh(1^+_{gs})$	$\rightarrow$ β^-	$Pd(2^+_2)$	0.9312	0.56	6.0	6.43
108	$Ag(1^+_{gs})$	$\rightarrow$ β^+/EC	$Pd(2^+_1)$	0.4339	0.56	5.46	5.20
	$Ag(1^+_{gs})$	$\rightarrow$ β^+/EC	$Pd(0^+_2)$	1.0528	0.56	4.89	5.24

Continued on next page

Table 6 – *Continued from previous page*

A	Process			E_f (MeV)	g_A	$\log ft_{exp}$	$\log ft_{th}$
108	$Ag(1^+_{gs})$	$\rightarrow$ β^+/EC	$Pd(2^+_2)$	0.9312	0.56	—	6.03
108	$Ag(1^+_{gs})$	$\rightarrow$ β^-	$Cd(2^+_1)$	0.6330	0.56	5.35	5.97
110	$Ag(1^+_{gs})$	$\rightarrow$ β^-	$Cd(2^+_1)$	0.6578	0.60	5.524	5.75
	$Ag(1^+_{gs})$	$\rightarrow$ β^-	$Cd(0^+_2)$	1.4731	0.60	6.80	5.55
	$Ag(1^+_{gs})$	$\rightarrow$ β^-	$Cd(2^+_2)$	1.4758	0.60	7.35	7.47
112	$In(1^+_{gs})$	$\rightarrow$ β^+/EC	$Cd(2^+_1)$	0.6175	0.64	5.309	5.14
	$In(1^+_{gs})$	$\rightarrow$ β^+/EC	$Cd(0^+_2)$	1.2245	0.64	5.376	5.66
	$In(1^+_{gs})$	$\rightarrow$ β^+/EC	$Cd(2^+_2)$	1.3124	0.64	7.17	6.48
114	$Ag(1^+_{gs})$	$\rightarrow$ β^-	$Cd(2^+_1)$	0.5585	0.68	5.6	5.99
	$Ag(1^+_{gs})$	$\rightarrow$ β^-	$Cd(0^+_2)$	1.1345	0.68	6.3	5.49
	$Ag(1^+_{gs})$	$\rightarrow$ β^-	$Cd(2^+_2)$	1.2097	0.68	6.5	7.87
114	$In(1^+_{gs})$	$\rightarrow$ β^+/EC	$Cd(2^+_1)$	0.5585	0.68	≥ 5.3	4.84
	$In(1^+_{gs})$	$\rightarrow$ β^+/EC	$Cd(0^+_2)$	1.1345	0.68	5.5	5.95
	$In(1^+_{gs})$	$\rightarrow$ β^+/EC	$Cd(2^+_2)$	1.2097	0.68	—	6.70
114	$In(1^+_{gs})$	$\rightarrow$ β^-	$Sn(2^+_1)$	1.2999	0.68	5.58	5.20

Continued on next page

Table 6 – *Continued from previous page*

A	Process			E_f (MeV)	g_A	$\log ft_{exp}$	$\log ft_{th}$
116	$In(1^+_{gs})$	$\rightarrow$ β^-	$Sn(2^+_1)$	1.2935	0.72	5.85	5.52
	$In(1^+_{gs})$	$\rightarrow$ β^-	$Sn(0^+_2)$	1.7569	0.72	5.88	6.64
	$In(1^+_{gs})$	$\rightarrow$ β^-	$Sn(2^+_2)$	2.1123	0.72	6.31	7.25
118	$In(1^+_{gs})$	$\rightarrow$ β^-	$Sn(2^+_1)$	1.2297	0.76	5.63	5.53
	$In(1^+_{gs})$	$\rightarrow$ β^-	$Sn(0^+_2)$	1.7583	0.76	5.98	6.32
	$In(1^+_{gs})$	$\rightarrow$ β^-	$Sn(2^+_2)$	2.0429	0.76	6.15	6.96
118	$Sb(1^+_{gs})$	$\rightarrow$ β^+/EC	$Sn(2^+_1)$	1.2297	0.76	5.79	5.58
	$Sb(1^+_{gs})$	$\rightarrow$ β^+/EC	$Sn(0^+_2)$	1.7583	0.76	5.69	6.89
	$Sb(1^+_{gs})$	$\rightarrow$ β^+/EC	$Sn(2^+_2)$	2.0429	0.76	6.84	7.81
120	$In(1^+_{gs})$	$\rightarrow$ β^-	$Sn(2^+_1)$	1.1713	0.80	5.23	5.58
	$In(1^+_{gs})$	$\rightarrow$ β^-	$Sn(0^+_2)$	1.8753	0.80	5.96	6.29
	$In(1^+_{gs})$	$\rightarrow$ β^-	$Sn(2^+_2)$	2.0972	0.80	6.37	6.93
122	$In(1^+_{gs})$	$\rightarrow$ β^-	$Sn(2^+_1)$	1.1405	0.60	5.36	5.87
	$In(1^+_{gs})$	$\rightarrow$ β^-	$Sn(0^+_2)$	2.0877	0.60	6.49	6.52
	$In(1^+_{gs})$	$\rightarrow$ β^-	$Sn(2^+_2)$	2.1538	0.60	5.71	7.16

Continued on next page

Table 6 – *Continued from previous page*

A	Process			E_f (MeV)	g_A	$\log ft_{exp}$	$\log ft_{th}$
122	$I(1^+_{gs})$	$\rightarrow$ β^+/EC	$Te(2^+_1)$	0.5641	0.60	5.39	6.94
	$I(1^+_{gs})$	$\rightarrow$ β^+/EC	$Te(0^+_2)$	1.3574	0.60	5.93	6.56
	$I(1^+_{gs})$	$\rightarrow$ β^+/EC	$Te(2^+_2)$	1.2570	0.60	6.31	7.81
124	$Cs(1^+_{gs})$	$\rightarrow$ β^+/EC	$Xe(2^+_1)$	0.3540	0.63	5.10	5.98
	$Cs(1^+_{gs})$	$\rightarrow$ β^+/EC	$Xe(2^+_2)$	0.8465	0.63	5.89	7.14
126	$Cs(1^+_{gs})$	$\rightarrow$ β^+/EC	$Xe(2^+_1)$	0.3886	0.67	5.151	5.77
	$Cs(1^+_{gs})$	$\rightarrow$ β^+/EC	$Xe(0^+_2)$	1.3139	0.67	5.39	6.52
	$Cs(1^+_{gs})$	$\rightarrow$ β^+/EC	$Xe(2^+_2)$	0.8799	0.67	5.78	7.23
128	$I(1^+_{gs})$	$\rightarrow$ β^+/EC	$Te(2^+_1)$	0.7432	0.70	6.007	5.92
128	$I(1^+_{gs})$	$\rightarrow$ β^-	$Xe(2^+_1)$	0.4429	0.70	6.495	5.92
	$I(1^+_{gs})$	$\rightarrow$ β^-	$Xe(0^+_2)$	1.5830	0.70	7.748	5.46
	$I(1^+_{gs})$	$\rightarrow$ β^-	$Xe(2^+_2)$	0.9695	0.70	6.754	6.79
128	$Cs(1^+_{gs})$	$\rightarrow$ β^+/EC	$Xe(2^+_1)$	0.4429	0.70	5.093	5.71
	$Cs(1^+_{gs})$	$\rightarrow$ β^+/EC	$Xe(0^+_2)$	1.5830	0.70	5.583	6.84
	$Cs(1^+_{gs})$	$\rightarrow$ β^+/EC	$Xe(2^+_2)$	0.9695	0.70	5.832	7.47

Continued on next page

Table 6 – *Continued from previous page*

A	Process			E_f (MeV)	g_A	$\log ft_{exp}$	$\log ft_{th}$
130	$Cs(1^+_{gs})$	$\rightarrow$ β^+/EC	$Xe(2^+_1)$	0.5361	0.73	6.3	5.65
	$Cs(1^+_{gs})$	$\rightarrow$ β^+/EC	$Xe(0^+_2)$	1.7935	0.73	7.0	7.16
	$Cs(1^+_{gs})$	$\rightarrow$ β^+/EC	$Xe(2^+_2)$	1.1221	0.73	7.5	7.74
134	$La(1^+_{gs})$	$\rightarrow$ β^+/EC	$Ba(2^+_1)$	0.6047	0.80	5.99	5.40
	$La(1^+_{gs})$	$\rightarrow$ β^+/EC	$Ba(0^+_2)$	1.7606	0.80	7.32	7.36
	$La(1^+_{gs})$	$\rightarrow$ β^+/EC	$Ba(2^+_2)$	1.1680	0.80	7.31	7.83

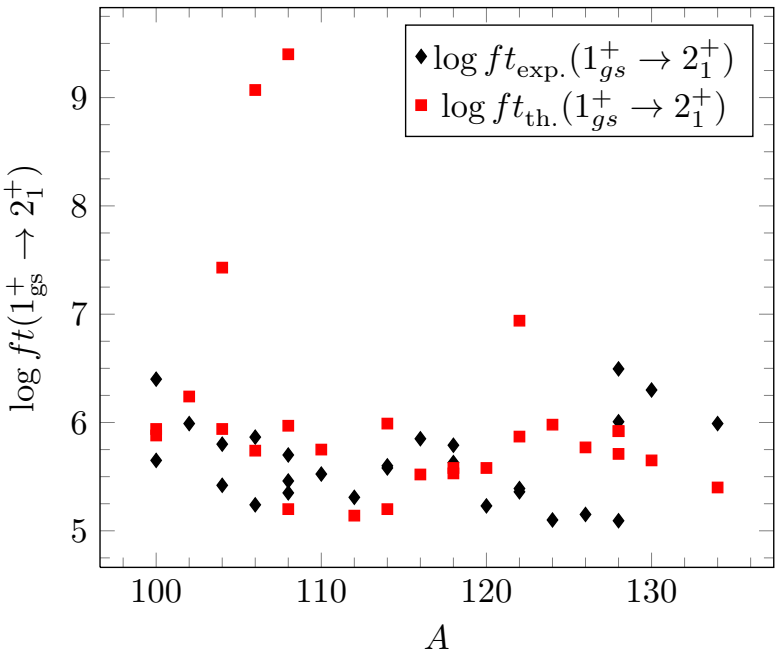

Figure 7: Experimental and theoretical $\log ft$ values of decays to the first excited 2^+ states of the even-even nuclei.

A curious case arises in the decay of rhodium to palladium via β^- decay, in

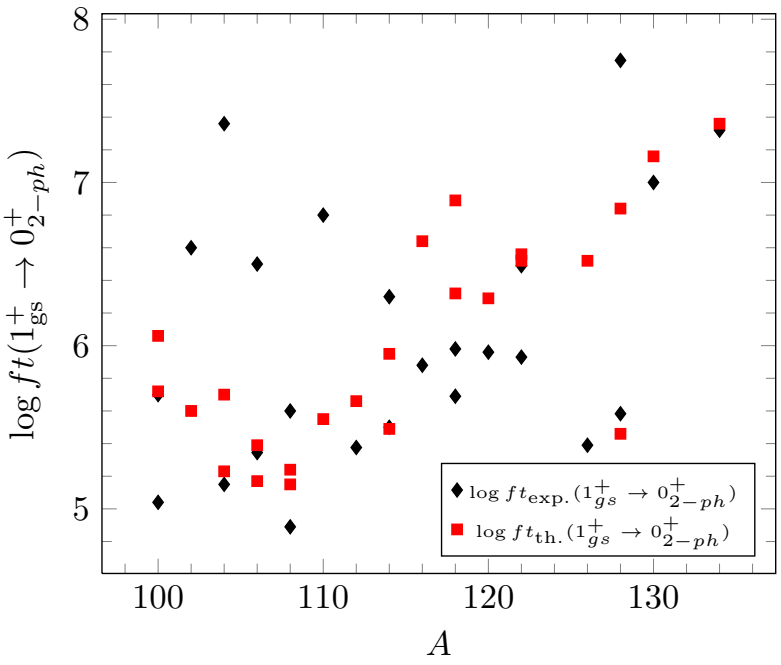

Figure 8: Experimental and theoretical $\log ft$ values of decays to the 0^+ quadrupole two-phonon states of the even-even nuclei.

which the transition to the first 2^+ state is predicted very slow for each $A = 104, 106, 108$. This can be seen in Figure 7 as the largest deviations from the experimental values. The deviation is likely to be due to the X and Y amplitudes in the major components of the wave function of the ground state of the Rh nucleus having opposite sign. There are thus large cancellations in the transition amplitudes and the calculated $\log ft$ values are very high making the comparative half lives too long by several orders of magnitude. It might also hint that the QRPA wave function of the first 2^+ state does not connect with the corresponding experimental state.

It is often not clear which states in the experimental spectrum actually correspond to the excited two-phonon states calculated from equation (8). There might be two 2^+ states accompanied by a 0^+ state within an essentially degenerate small energy interval. The degeneracy of the quadrupole two-phonon triplet might also be split by an unexpectedly large amount in the experimental spectrum. There are cases like this in the $A = 116 - 118$ processes involving isotopes of Sn. Sn has a magic proton number of 50, which leads to the energy of the first excited 2^+ state to be high compared to other neighbouring isotopes. This then leads to the two-phonon states to have a higher energy and thus makes it easier for them to get mixed with other kinds of excited states.

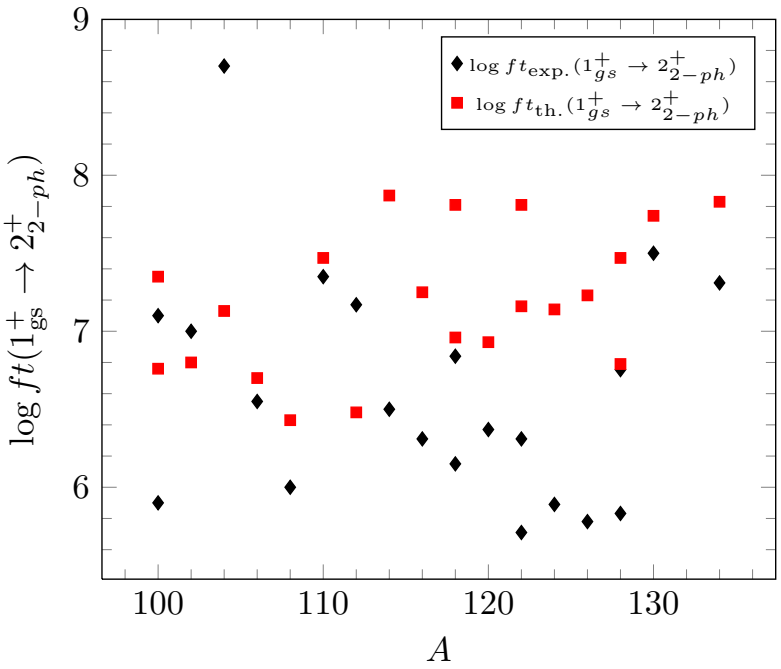

Figure 9: Experimental and theoretical $\log ft$ values of decays to the 2^+ quadrupole two-phonon states of the even-even nuclei.

The experimental $\log ft$ values for these states are rather similar, though, so the error brought by a mistaken two-phonon state is not very substantial. The states appearing on Table 6 are ones thought of as the most reasonable guesses.

A disappearance of a clear two-phonon 0^+ state happens at $A \geq 126$. The experimental $\log ft$ values are given for the lowest excited 0^+ state, but this state is always too high in energy to be the two-phonon state the theory predicts. Either the degeneracy of the collective two-phonon triplet increases with increasing mass number A or the formation of this particular multipolarity is prevented in nuclei investigated here with $A \geq 126$. The theoretical $\log ft$ values for these transitions often seem to deviate more than one unit from the experimental $\log ft$ value for the 0^+_2 state. There are also a few cases in which the theoretical prediction would coincide almost perfectly with the experimental value for the 0^+_2 state. Predictions of $\log ft$ values in the QRPA framework are often a game of chance in single events and it would take a larger specimen of nuclei and processes to make definite conclusions on the matter. The 4^+ state of the supposed quadrupole two phonon triplet can nevertheless be found, as is the case in the experimental energy spectra of ^{126}Xe and ^{128}Xe in Figure 10. The first excited 0^+ state in these cases lies around triple the energy of the first

2^+ state. This makes it more probable for the 0_2^+ state to result from some other origin than two quadrupole phonons.

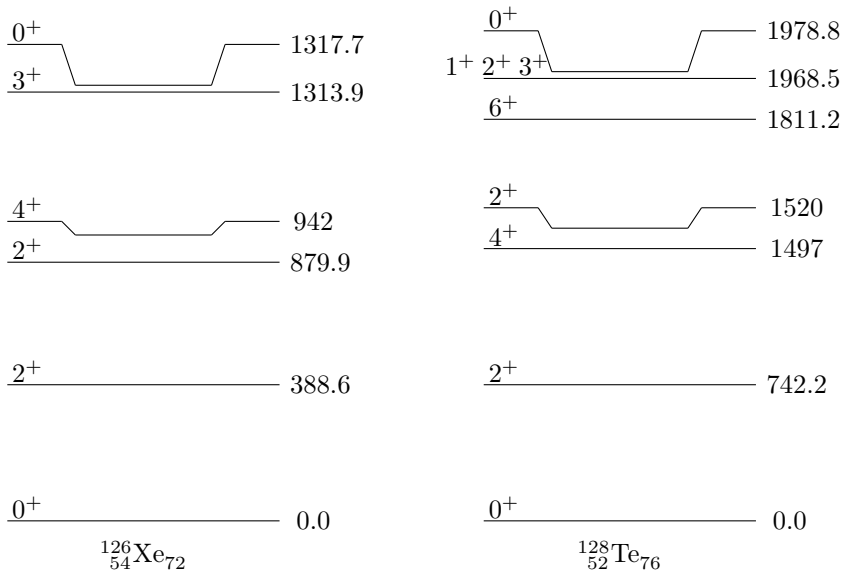

Figure 10: The experimental low energy spectra of ^{126}Xe and ^{128}Xe [12]. The energies are in keV. The 2^+ and 4^+ members of the quadrupole two-phonon triplets can be recognized at around twice the energy of the first 2^+ state, but the first 0^+ state is much higher in energy.

4 Conclusions

A study of beta decay properties in the QRPA framework was performed in a vast mass region $A = 100 - 134$ in order to understand the systematics of the effective axial-vector coupling constant g_A in allowed Gamow-Teller transitions. The investigated processes were transitions to and from the ground states of the following odd-odd nuclei: ^{100}Nb, ^{100}Tc, ^{102}Tc, ^{104}Rh, ^{106}Rh, ^{106}Ag, ^{108}Rh, ^{108}Ag, ^{110}Ag, ^{112}In, ^{114}Ag, ^{114}In, ^{116}In, ^{118}In, ^{118}Sb, ^{120}In, ^{122}In, ^{122}I, ^{124}Cs, ^{126}Cs, ^{128}I, ^{128}Cs, ^{130}Cs and ^{134}La. Calculations were made in the QRPA framework in large valence spaces using realistic Bonn-A two-body interactions.

First, the ground state to ground state decays were examined by fitting the theoretical geometric means of the left and right Gamow-Teller matrix elements associated with each odd-odd nucleus to an experimental theoretical mean. This was done using four separate values for the particle-particle interaction strength parameter $g_{pp} = 0.6,\ 0.7,\ 0.8,\ 0.9$. The results were plotted to a graph, which is presented in Figure 6. In the graph, there were two mass regions in which the average behaviour of g_A was roughly linear. By this method, a linear model for the behaviour of g_A as a function of the mass number A was adopted and predictions were made for the $\log ft$ values of ground state to ground state decays with an average value of $g_{pp} = 0.7$ and

$$g_A = \begin{cases} 0.02A - 1.6, & \text{for} A \in [100,\ 120] \\ \frac{1}{60}A - \frac{43}{30}, & \text{for} A \in [122,\ 134] \end{cases}.$$

This examination left little doubt as to whether an effective value for g_A is needed as the results all around pointed to values less than unity. With a linear model suggested to depict the behaviour of the effective g_A, the model was then put to a test. The linear model for g_A was found accurate in describing the ground state to ground state decays. The mean deviation of theoretical $\log ft$ values from experimental ones with all processes included was 0.23. Much of the deviation is attributed to the decays which were furthest away from the linear fit of Figure 6. The linear model gives very good predictions for such a simple model.

The study was then extended to decays from the 1^+ ground state of the odd-odd nuclei to the lowest lying excited states in the even-even nuclei: the first excited 2^+ state and the collective quadrupole two-phonon 0^+ and 2^+ states. Predictions of $\log ft$ values were made for every process with experimental reference data available.

The accuracy of the predictions for decays to the first 2^+ states was decent, yet somewhat expectedly not as good as in the case of ground state decays. The decay of rhodium 1^+_{gs} to palladium 2^+_1 yielded a very high theoretical $\log ft$ value for each $A = 104, 106, 108$. This was attributed to unfortunate cancellations in the transition amplitudes due to the X and Y amplitudes of the wave function of the 1^+ ground state of the rhodium nucleus. All other theoretical values were within reasonable limits of the experimental values. In any case, the linear g_A model gives better overall predictions than a single constant value for g_A.

The predictions to the two-phonon states act as just that: predictions. It is difficult to make any definite conclusions based on the calculations presented here. The transitions to the 2^+_{2-ph} states are systematically predicted too slow except on a few occasions. On the decays to 0^+_{2-ph} states there is more variance. It is also often difficult to be sure if a state in the experimental spectrum is actually a two-phonon state. In the spectra of tin isotopes, there are a lot of 2^+ states around the expected energy of the two-phonon triplet. There is not much variance in the experimental $\log ft$ values to these states making this beta decay property a bad indicator of a two-phonon state. There is a curious disappearance of the two-phonon 0^+ states in the experimental spectra of even-even nuclei with $A \geq 126$. Either the degeneracy of the triplet is badly broken or, as the beta decay results and the fact that a 2^+ and a 4^+ state are still found at the expected energy of the two-phonon triplet would hint, the 0^+ state of the triplet does not form.

The linear model for g_A has deemed successful in predicting single beta decays from ground state to ground state as well as decays to the first excited 2^+ state of the even even nuclei. The next step would be to apply the model to the study of double beta decay. Predictions can be made for each possible two neutrino double beta decay in the investigated mass region and compare with available experimental data. It would also help to have good predictions for processes still lacking experimental data. The results are expected to be in good agreement with experiment.

References

[1] J. Suhonen: *From Nucleons to Nucleus: Concepts of Microscopic nuclear Theory* (Springer Berlin Heidelberg, 2007)

[2] J. Suhonen, O. Civitarese: Probing the quenching of g_A by single and double beta decays, Phys. Lett. B **725**, 153 (2013)

[3] J. D. Holt, J. Engel: Effective double-β-decay operator for ^{76}Ge and ^{82}Se, Phys. Rev. C **87**, 064315 (2013)

[4] J. Barea, J. Kotila, F. Iachello: Nuclear matrix elements for double-β decay, Phys. Rev. C **87**, 014315 (2013)

[5] M. Baranger: Extension of the Shell Model for Heavy Spherical Nuclei, Phys. Rev. **120**, 957 (1960)

[6] J. Suhonen, O. Civitarese: Double-beta-decay nuclear matrix elements in the QRPA framework, J. Phys. G: Nucl. Part. Phys. **39**, 085105 (2012)

[7] M. Goeppert-Meyer: Double Beta-Disintegration, Phys. Rev. **48**, 512 (1935)

[8] J. Bardeen, L. N. Cooper, J. R. Schrieffer: Theory of Superconductivity, Phys. Rev. **108**, 1175 (1957)

[9] J. Suhonen: Calculation of allowed and first-forbidden beta-decay transitions of odd–odd nuclei, Nucl. Phys. A **563**, 205 (1993)

[10] D. J. Rowe: Equations-of-Motion Method and the Extended Shell Model, Rev. Mod. Phys **40**, 153 (1968)

[11] R. F. Casten, N. V. Zamfir: Evidence for pervasive phonon structure of nuclear excitations, Phys. Rep. **264**, 81 (1996)

[12] National Nuclear Data Center, http://www.nndc.bnl.gov/ (2014)

[13] J. Suhonen, O. Civitarese: Systematic QRPA study of β^- and β^+/EC decay transitions to excited states of $^{110-114}$Cd and $^{114-122}$Sn, Nucl. Phys. A **584**, 449 (1995)

[14] J. Suhonen, O. Civitarese: Effects of orbital occupancies and spin–orbit partners on $0\nu\beta\beta$-decay rates, Nucl. Phys. A **847**, 207 (2010)

[15] J. Suhonen, T. Taigel, A. Faessler: pnQRPA calculation of the β^+/EC quenching for several neutron-deficient nuclei in mass regions A = 94–110 and A = 146–156, Nucl. Phys. A **486**, 91 (1988)

[16] P. Pirinen: Beta decay properties and effective axial-vector coupling in ground state to ground state decays of mass region A = 100 - 134 isotopes, Research training, University of Jyväskylä (2014)

[17] O. Civitarese, J. Suhonen: Strength of $J^\pi = 1^+$ Gamow-Teller and isovector spin monopole transitions in double-β-decay triplets, Phys. Rev. C **89**, 044319 (2014)

[18] A. Bohr, B.R. Mottelson: *Nuclear Structure, Vol. 1* (Benjamin, New York, 1969)

[19] A. H. Wapstra, G. Audi: The 1983 atomic mass evaluation: (I). Atomic mass table, Nucl. Phys. A **432**, 1 (1985)

[20] Kenneth S. Krane: *Introductory Nuclear Physics* (John Wiley & Sons, 1987)

[21] E. Fermi: An attempt of a theory of beta radiation I, Z. Phys. **88**, 161 (1934)

[22] G. Gamow, E. Teller: Selection Rules for the β-Disintegration, Phys. Rev. **49**, 895 (1936)

[23] N. N. Bogoliubov: A new method in the theory of superconductivity I, Sov. Phys. JETP **7**, 41 (1958)

[24] J. G. Valatin: Generalized Hartree-Fock Method, Phys. Rev. **122**, 1012 (1961)

[25] J. Suhonen, private communication (2014)

[26] C. M. Lederer, V. S. Shirley et al.: *Table of Isotopes, Seventh Edition* (J. Wiley & Sons, 1978)